

Article

# Implementation of Single Phase Soft Switched PFC Converter for Plug-in-Hybrid Electric Vehicles

Aiswariya Sekar \* and Dhanasekaran Raghavan

Received: 22 September 2015 ; Accepted: 10 November 2015 ; Published: 18 November 2015  
Academic Editor: K. T. Chau

Syed Ammal Engineering College, Ramanathapuram 623502, India; rdhanashekar@yahoo.com

\* Correspondence: aiswariyasekar@yahoo.co.in; Tel.: +91-94-8800-6122

**Abstract:** This paper presents a new soft switching boost converter with a passive snubber cell without additional active switches for battery charging systems. The proposed snubber finds its application in the front-end ac-dc converter of Plug-in Hybrid Electric Vehicle (PHEV) battery chargers. The proposed auxiliary snubber circuit consists of an inductor, two capacitors and two diodes. The new converter has the advantages of continuous input current, low switching stresses, high voltage gain without extreme duty cycle, minimized charger size and charging time and fewer amounts of cost and electricity drawn from the utility at higher switching frequencies. The switch is made to turn ON by Zero Current Switching (ZCS) and turn OFF by Zero Voltage Switching (ZVS). The detailed steady state analysis of the novel ac-dc Zero Current- Zero Voltage Switching (ZC-ZVS) boost Power Factor Correction (PFC) converter is presented with its operating principle. The experimental prototype of 20 kHz, 100 W converter verifies the theoretical analysis. The power factor of the prototype circuit reaches near unity with an efficiency of 97%, at nominal output power for a  $\pm 10\%$  variation in the input voltage and  $\pm 20\%$  variation in the snubber component values.

**Keywords:** boost converter; electric vehicles; soft switching; PFC; ZCS; ZVS

## 1. Introduction

Plug-in Hybrid Electric Vehicles (PHEVs) are hybrid electric vehicles containing batteries that are rechargeable and restorable to complete charge by connecting the plug of vehicle to an external electric power source. PHEVs and Electric Vehicles (EVs) are becoming more popular with users and manufacturers. Power Factor Correction (PFC) is vital to meet the effectiveness and restrictive standards for the ac supply mains. Because of the constrained space in vehicles and expanding power intake, chargers are required to convey more power with little volume. The most well-known charger power architecture incorporates an ac-dc converter with PFC followed by an isolated dc-dc converter [1–5]. During the most recent decade, numerous standards were introduced for ac-dc converters in order to draw pure sinusoidal currents from the utilities [6,7]. Mostly they involve a diode rectifier at the front end leading to harmonics in the input current waveform. In order to shape the input current to be sinusoidal and thereby to improve the power factor, PFC is required. PFC can be of two types. Passive PFC is low cost since it does not require active switches and complex control circuits but it cannot provide high power factors like active PFC, so the active type is widely applied for PFC. Various active PFC methodologies are available for boost circuits to bring high power factor ability with ease of control attracting more research on this topic [8–11].

Due to the presence of parasitic components in the conventional boost converter the output voltage cannot be more than six times that of the applied voltage. Also when it is operated with high duty cycle the overall efficiency is reduced with increased Electro-Magnetic Interference (EMI) due to the reverse recovery problems in the diode [12]. Metal Oxide Semiconductor Field Effect Transistor

(MOSFET) switches experience high voltage and current stresses [13]. The input current ripple is large and this will lessen the efficiency of the system [14].

Many researches have been carried out to enhance the efficiency of the dc-dc converter. Two boost converters were interleaved to reduce the input current ripple and the switching losses with high voltage gain [15,16]. But in the applications involving high voltage, the efficiency was limited and the control was complex hence it suffers from voltage stress like that of conventional converters [17]. Cascading of boost converters does not work well due to the boost diode reverse recovery problems in the case of high output applications. To overcome these drawbacks a quadratic converter obtained by integration of two switches was proposed [18].

A sliding mode controller-based quadratic boost converter was analyzed and its efficiency was evaluated and presented in [19]. For a Zero Current-Zero Voltage Switching (ZC-ZVS) quadratic converter proposed in [20] the voltage stress in the switch was nearly same as that of the output voltage, and the current stress leads to higher conduction losses and reduced efficiency. When coupled inductors were used to achieve high voltage gain the leakage inductance losses degraded the system efficiency [21]. To recycle the leakage energy active clamp circuits were used which increased the overall cost and complexity of the structure [22]. It produced pulsated input currents. The resonance created between the parasitic capacitor of the boost diode and the leakage inductance of the coupled inductor necessitated the use of switches with high voltage ratings. Input filters are mandatory to reduce the input current ripples when the turn cycle of the coupled inductor was raised to increase the output voltage [23].

In [24], a single coupled inductor was formed by integrating the boost inductor with the transformer of the fly back converter. The advantage obtained was the achievement of high voltage gain. When a switched capacitor is integrated with a coupled inductor the leakage energy of the coupled inductor was recycled thereby reducing the voltage stress [25]. Capacitor diode voltage multiplier cells increase the voltage gain but with increased overall system cost [26]. The proposed topology in [27] degraded the voltage stress with improved voltage gain, but with additional semiconductor components, increased size and cost, reduced efficiency and it had floating output. In [24–27], the proposed converters required a large input filter in order to reduce the pulsating current ripple and experienced EMI noise problems. The circuit that combined the coupled inductor and voltage doubler cell structure reduced high input current ripple with two switches which increased the control complexity [28]. Active snubbers minimized the switching losses by means of auxiliary switches. Unfortunately, the auxiliary switch increased the complexity of both the power and control circuits [29–32].

A passive lossless snubber had quite simply restricted switching losses and EMI noise utilizing no active elements and no power dissipative elements. No additional control was required and no circulating energy was produced. The circuit structure was very simple like a RCD snubber while the power was as high as that of an active snubber and resonant converter. Less cost, excellent performance, and high reliability were the particular advantages of a passive lossless snubber [33,34]. The passive snubber circuits that were used for a basic PFC converter [35,36], a three level PFC converter [37] and a bridgeless PFC converter [38] consist of a flying capacitor in addition to snubber capacitors, inductors, and diodes. These snubber circuits act as turn ON snubbers since they recover the stored energy of the main switch with the help of the additional series-connected inductor. These circuits cannot help during turn OFF. The turn OFF passive snubber proposed for the main switch was composed of resistor, capacitor and diode components to reduce the rise of the switch voltage [39], but the snubber resistor introduced power losses to the total loss thus degrading the circuit efficiency. In order to reduce the reverse recovery current of the output diodes, a passive snubber circuit comprised of saturable inductors was used [40,41]. Unfortunately this increased the voltage stress of the main switch with additional cost of inductors. In [42] a snubber circuit with a saturable inductor was used to lower the reverse recovery current of the output diodes. Even though the problem of additional voltage stress of the main switch had been eliminated by the snubber, the main drawback was that

the three additional inductors of the snubber circuit increased the circuit size because of the nine additional passive components. A Ripple Mirror (RM) circuit was proposed for a boost converter to reduce the ripple. Boundary mode control was presented and the converter achieved ZVS and ZCS conditions. At rated load, the circuit had an efficiency of 93% [43].

To charge a plug-in-electric vehicle (PEV) efficiently a new dc power micro grid architecture was proposed and evaluated. The improvement in efficiency and reduction in complexity were gained since the PEV was coupled directly with the dc link without a static converter [44]. An onboard charger based on buck converter was proposed with ZCS for PEV. The controller used both pulse frequency modulation and pulse width modulation methods to achieve high efficiency and high power density with reduced input current THD [45]. In [46], a ZVS forward converter was implemented in the power supply system for hybrid renewable energy conversion. ZVS has reduced the switching and conduction losses for the active switches.

This paper is organized as follows: Section 2 presents a review of existing ac-dc PFC converters and Section 3 presents the proposed circuit configuration and operating principle in Continuous Conduction Mode (CCM). Section 4 gives the design guidelines with an illustrative example. The experimental results of a 100 W, 24  $V_{ac}$  input/40  $V_{dc}$  output prototype of the ac-dc boost PFC converter with  $f_s = 20$  kHz are given in Section 5 to verify the feasibility of the proposed snubber. Finally, the conclusions drawn from this work are presented in Section 6.

### 2. Review of Existing ac-dc PFC Boost Topologies

The conventional boost topology is the most well-known topology for PFC applications. In PFC applications, a diode bridge is utilized to rectify the ac input voltage to dc, and this is followed by the boost converter, as shown in Figure 1a.

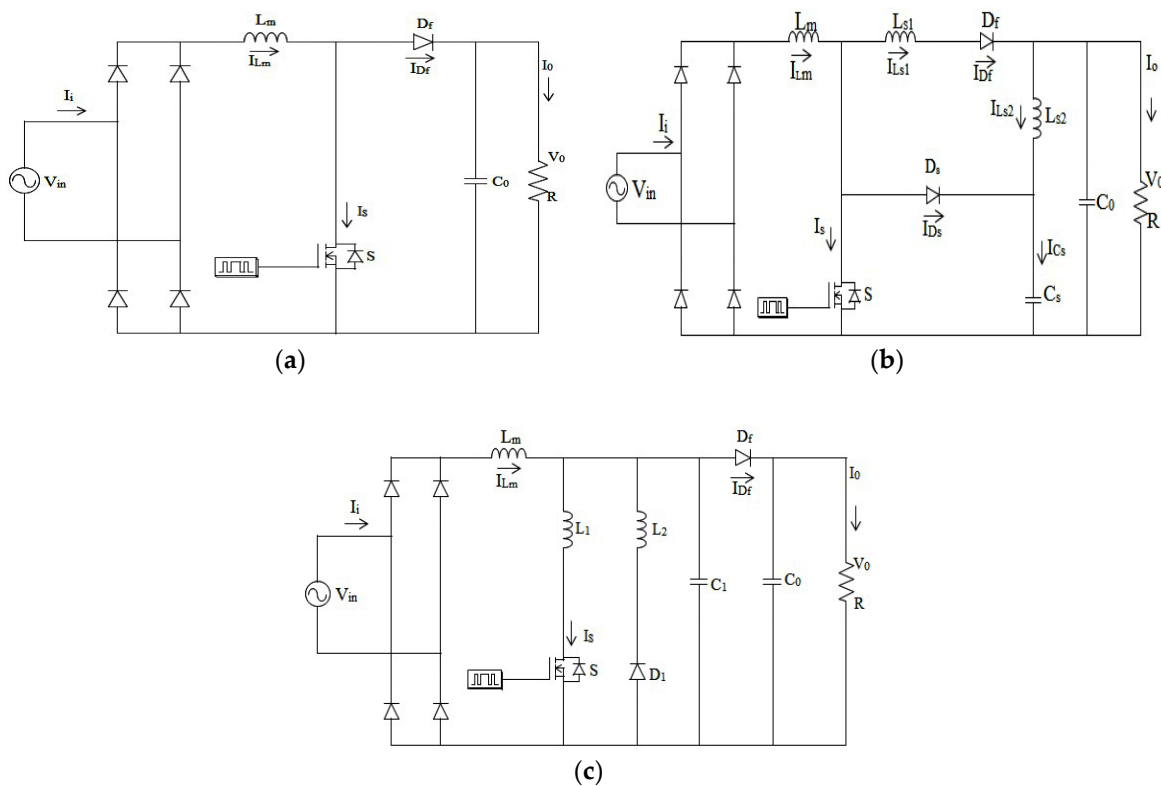


**Figure 1.** Existing ac-dc Boost Power Factor Correction (PFC) Topologies. (a) Conventional ac-dc Boost PFC Converter; (b) ac-dc Boost PFC Converter Passive Snubber [33]; (c) ac-dc Boost PFC Converter with Passive Snubber [34].

Be that as it may, this topology has its downsides, which are high input current ripple, high switching and conduction losses and reduced efficiency at higher power levels because of the diode bridge losses. The boost converter topology with passive snubber [33] achieved soft switching characteristic of the main switch with ZCS turn ON and ZVS turn OFF with the addition of two inductors, one diode and one capacitor as shown in Figure 1b. This avoids the degradation of efficiency with reduction in the diode losses, yet has some input current ripple problems. The passive boost converter snubber circuit [34], as shown in Figure 1c achieved ZCS turn ON and ZCS turn OFF of the main switch and reduces the problem of input current ripple and switching losses, but it still had the problem of lower efficiency for a vehicle charger system. In order to achieve high efficiency at light loads and low ac input lines so as to minimize the charger size and charging time and to lessen the amount and cost of electricity drawn from the utility, a new passive snubber circuit has been proposed in this paper.

### 3. Circuit Structure of Proposed PFC Converter

The proposed LCD passive snubber consists of a snubber inductor  $L_s$ , snubber capacitors  $C_1$  and  $C_2$  and snubber diodes  $D_1$  and  $D_2$  as in Figure 2. The LCD snubber is added to the conventional hard switched boost PFC converter circuit which comprises of an input inductor  $L_m$ , output capacitor  $C_0$ , main diode  $D_f$  and a switch  $S$ .

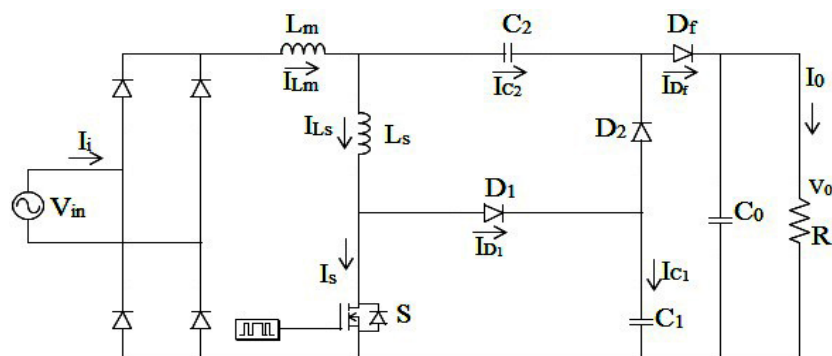
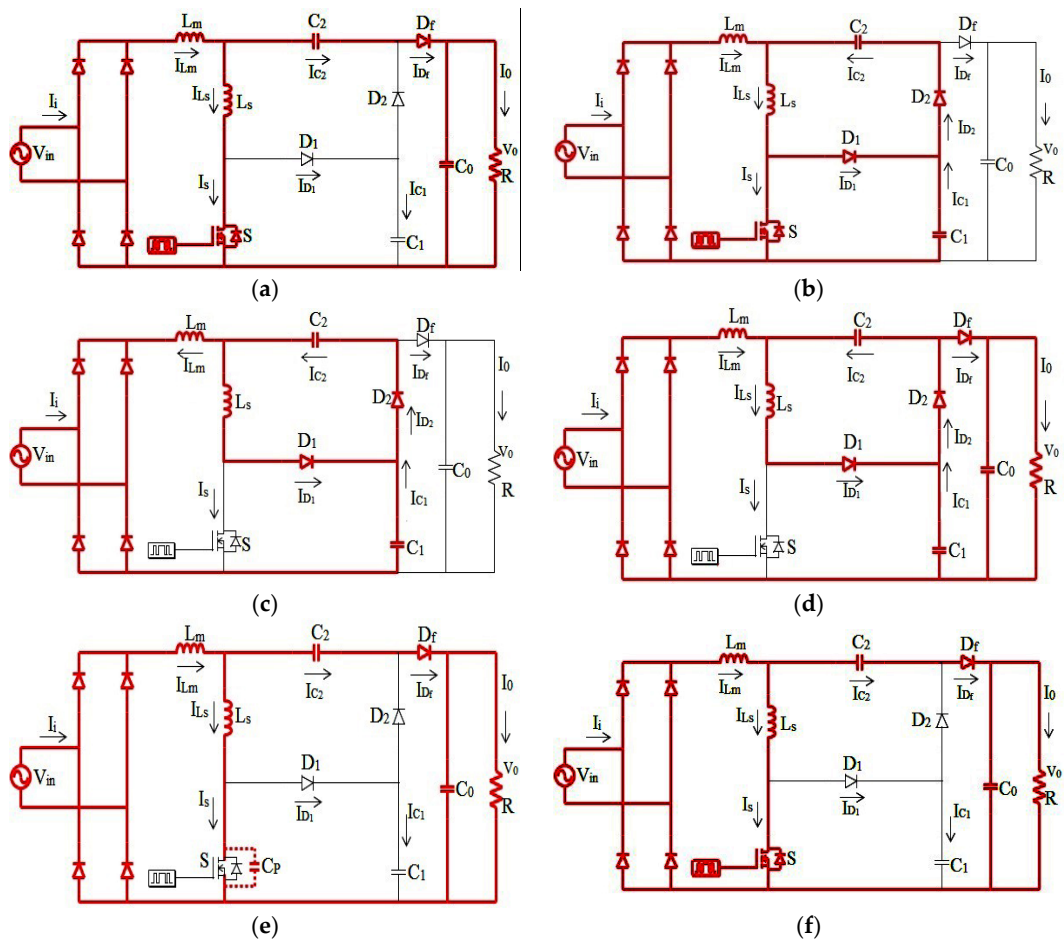


Figure 2. Proposed Boost PFC Converter.

#### 3.1. Operating Principle

One switching period of the proposed converter has six operating modes. They are explained by the equivalent circuit of proposed converter as in Figure 3. The key waveforms of the ac-dc PFC boost converter are shown in Figure 4. Some assumptions are made during the simulation of proposed converter:

- All the semiconductor devices used in the proposed converter are ideal.
- Reverse recovery of the boost converter diode is considered and taken into account.
- The output capacitor  $C_0$  is assumed to be large to produce a constant output voltage.
- The main inductor  $L_m$  is much greater than snubber inductor  $L_s$  to have a constant input current.



**Figure 3.** Operation modes of the proposed converter in a switching cycle: (a) mode 1; (b) mode 2; (c) mode 3; (d) mode 4; (e) mode 5; (f) mode 6.

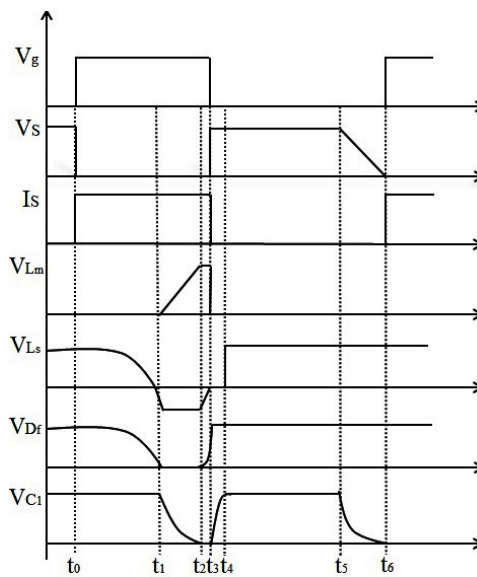


**Figure 4.** Typical waveforms concerning the operation stages for the converter operating in Continuous Conduction Mode (CCM).

### 3.1.1. Mode 1 ( $t_0 < t < t_1$ )

Switch S is turned ON at  $t = t_0$ . Diodes  $D_1$  and  $D_2$  are in the OFF state. The main diode  $D_f$  remains ON. The voltage across the snubber capacitor  $C_1$  reaches the output voltage level. During this mode the current through  $L_m$  and switch S is given by:

$$I_{L_m}(t) = I_{L_m}(t_0) - \frac{(V_0 - V_{in} - V_{C_2})}{L_m}(t - t_0) \quad (1)$$

$$I_s(t) = \frac{(V_0 - V_{C_2})}{L_s}(t - t_0) \quad (2)$$

Thus the switch is turned ON at the ZCS condition due to the diode current *i.e.*, given by:

$$I_{D_f} = I_{L_m} - I_s \quad (3)$$

$$I_{D_f}(t) = I_{L_m}(t_0) - \left( \frac{L_s(V_0 - V_{in} - V_{C_2}) + L_m(V_0 - V_{C_2})}{L_m L_s} \right) (t - t_0) \quad (4)$$

When the current through the diode  $D_f$  decreases to zero then

$$I_s(t_1) = I_{L_m}(t_1) \quad (5)$$

### 3.1.2. Mode 2 ( $t_1 < t < t_2$ )

During the beginning of this mode snubber diode  $D_2$  is turned ON,  $D_1$  is in the OFF state due to the turn OFF of the main diode  $D_f$  turn OFF, and switch S remains ON. A resonance starts between  $C_1, D_2, C_2, L_s$  and the switch. The voltage across the snubber capacitor  $C_1$  is given by:

$$V_{C_1}(t) = \left( V_0 - V_{C_2} - \frac{L_s V_{in}}{L_m + L_s} \right) \cos \omega_r (t - t_1) + \left( V_{C_2} + \frac{L_s V_{in}}{L_m + L_s} \right) \quad (6)$$

$$\omega_r \cong \sqrt{(L_m + L_s) / L_m L_s C_1} \quad (7)$$

The current through diode  $D_2$  is given by:

$$I_{D_2}(t) = \omega_r C_1 \left( V_0 - V_{C_2} - \frac{L_s V_{in}}{L_m + L_s} \right) \sin \omega_r (t - t_1) \quad (8)$$

The input current through the main inductor  $L_m$  is given by:

$$I_{L_m}(t) = I_{L_m}(t_0) + \frac{V_{in}}{L_m + L_s} (t - t_1) - \frac{1}{\omega_r L_m} \left( V_0 - V_{C_2} - \frac{L_s V_{in}}{L_m + L_s} \right) \sin \omega_r (t - t_1) \quad (9)$$

The switch current during this mode is:

$$I_s(t) = I_{L_s}(t) = I_{L_m}(t) + I_{D_2}(t) \quad (10)$$

At the end of this mode the snubber diode  $D_1$  turns ON and voltage across the snubber capacitor  $C_1$  reaches zero.

### 3.1.3. Mode 3 ( $t_2 < t < t_3$ )

At  $t = t_2$ , the snubber diode  $D_1$  is turned ON, the snubber diode  $D_2$  remains in ON state. Snubber capacitor  $C_1$  is discharged fully. The current through the snubber inductor and the main inductor becomes:

$$I_{L_s}(t) = I_{L_s}(t_2) - \frac{V_{C_2}}{L_s}(t - t_2) \quad (11)$$

$$I_{L_m}(t) = I_{L_m}(t_2) - \frac{V_{in} + V_{C_2}}{L_m}(t - t_2) \quad (12)$$

Current freewheels through  $C_1$ ,  $D_2$ ,  $C_2$  and  $L_m$  and  $V_{in}$ . At  $t = t_3$ , switch is turned OFF with ZVS condition.

### 3.1.4. Mode 4 ( $t_3 < t < t_4$ )

At  $t = t_3$ , switch S remains in OFF state with  $D_1$  and  $D_2$  remaining in ON state, and the main diode is turned ON. Snubber capacitor  $C_1$  is charged by the current through main inductor  $L_m$  through the diode  $D_1$ . The current through  $D_1$  is given as:

$$I_{D_1}(t) = I_{L_S}(t) = I_{L_S}(t_2) - \frac{V_{C_2}}{L_S}(t - t_2) \quad (13)$$

Resonance starts between  $C_1$ ,  $D_2$ ,  $C_2$ ,  $L_S$  and source:

$$I_{D_2}(t) = I_{D_1}(t) - I_{L_m}(t) \quad (14)$$

At  $t = t_4$ , voltage across  $C_1$  reaches near the output voltage.

### 3.1.5. Mode 5 ( $t_4 < t < t_5$ )

At  $t = t_4$ , main diode remains ON; switch S will be in OFF state. A resonant path is created by  $L_S$  and the parasitic capacitor  $C_p$  of switch S and diodes  $D_1$  and  $D_2$  are turned OFF:

$$V_S(t) = V_{C_1}(t) = V_0 \quad (15)$$

$$V_{L_S}(t) = -V_{C_2} \quad (16)$$

$$V_{L_m}(t) = V_{in} + V_{C_2} - V_0 \quad (17)$$

$$I_{L_m} = I_{D_f} \quad (18)$$

At  $t = t_5$ , the current through  $D_1$  and  $D_2$  reduce linearly to zero.

### 3.1.6. Mode 6 ( $t_5 < t < t_6$ )

At  $t = t_5$ , the main diode is in ON state, the switch S is remains in OFF state, and snubber diodes  $D_1$  and  $D_2$  are turned OFF as the current through them reduces to zero:

$$I_{L_m} = I_{D_f} \quad (19)$$

$$V_{L_S}(t) = 0 \quad (20)$$

$$V_{L_m}(t) = V_{in} + V_{C_2} - V_0 \quad (21)$$

$$V_S(t) = V_0 - V_{C_2} \quad (22)$$

The snubber inductor  $L_S$  and the parasitic capacitance of the converter switch S create a resonance condition. Because of this resonance, there will be a decrease in the switch voltage from the output voltage level. The next switching cycle starts at the end of this mode *i.e.*,  $t = t_6$ , where the switch S is turned ON again.

## 4. Design of Proposed LCD Snubber

### 4.1. Main Inductor $L_m$

The boost inductor  $L_m$  should be designed in such a way that the current that flows through it should be less than the current that it can withstand *i.e.* two times the maximum input current:

$$I_{L_m} \cong \frac{(V_0 - V_{in} - V_{C_2})(1 - d)}{L_m f_S} \quad (23)$$

Thus when  $f_s$  increases, the value of main inductor in the proposed circuit is decreased when compared to that in the conventional converter:

$$I_{L_m} = \frac{(V_0 - V_{in})(1-d)}{L_m f_s} \quad (24)$$

#### 4.2. Resonant Inductor $L_S$

For achieving ZCS turn ON of the switch, the required value of the snubber inductor is determined from the following equation:

$$L_S > L_{S, min} = \frac{(V_0 - V_{C_2}) t_r}{I_i} \quad (25)$$

where,  $t_r$  is the rise time of the switch current.

When the switch is turned ON at  $t = t_1$ , the reverse recovery current of the main diode  $D_f$  flows through the resonant inductor.  $(V_0 - V_{C_2})$  is the voltage to be absorbed by  $L_S$  to avail the ZCS condition to turn ON the switch  $S$ . When  $L_S$  increases, it will decrease the turn ON losses of the switch. Maximum inductance value of  $L_S$  is given as from:

$$L_S \leq L_{S, max} = \frac{(1-d) T_S V_{C_2}}{I_{L_S}(t_2)} \quad (26)$$

#### 4.3. Resonant Capacitors $C_1$ and $C_2$

To control the  $dv/dt$  of switch at turn OFF a snubber capacitor  $C_1$  is connected in parallel to the switch with the diode  $D_1$ . The minimum value of  $C_2$  depends on the output voltage as it will appear across  $C_1$  during the switch turn OFF:

$$C_1 > C_{1, min} = \frac{I_S(t_2) t_f}{2V_0} \quad (27)$$

where,  $t_f$  is the switch current fall time

When  $C_1$  increases the turn OFF losses of the switch decreases since the voltage across the switch decreases.

For ZVS turn OFF:

$$V_{C_1}(t_2) = 0 \quad (28)$$

From this maximum value of  $C_1$  is determined as:

$$C_1 < C_{1, max} = \frac{1}{L_S} \left[ \frac{t_2 - t_1}{\cos^{-1}(-V_{C_2}(V_0 - V_{C_2}))} \right]^2 \quad (29)$$

The value of  $C_2$  must be chosen such the voltage across  $C_2$  is greater than the ripple voltage:

$$V_{C_2} \ll V_{C_2} \quad (30)$$

## 5. Experimental Results and Discussions

The overall performance of the new passive snubber circuit is estimated with the prototype constructed according to Figure 5. The values of snubber components are determined using Equations (25)–(29). Before  $t = t_5$ , when  $L_S = 70 \mu\text{H}$ ,  $I_{L_S}$  reaches zero for ZCS turn ON, when  $C_1 = 4.3 \text{ nF}$ , ZVS turn OFF is achieved and when  $C_2 = 2.5 \mu\text{F}$ , the  $V_{C_2}$  ripple voltage is negligibly small. The converter is operated with an ac input voltage of  $V_{in} = 24\text{V}$  which is rectified and boosted to the output dc voltage of  $V_0 = 40\text{V}$  and  $P_0 = 100\text{W}$  at  $f_s = 20 \text{ kHz}$ .

The proposed converter waveforms (Figure 6a–e) verify the key waveforms (Figure 4) at  $t = 30 \text{ s}$ . The components used in the hardware implementation of the proposed boost PFC converter are summarized in Table 1 with a detailed description.

In the experimental waveforms of the converter switch shown, there is a slow increase in the switch current and voltage since  $L_S$  controls the turn ON  $di/dt$  of  $S$  and  $C_1$  controls the turn OFF

$di/dt$  of  $S$ . It thus proves that switch  $S$  is turned ON with ZCS. There is no overlap between voltage and current waveforms for the main switch  $S$ .

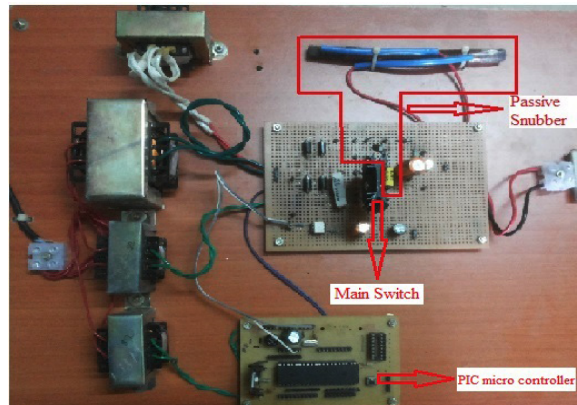


Figure 5. Prototype model.

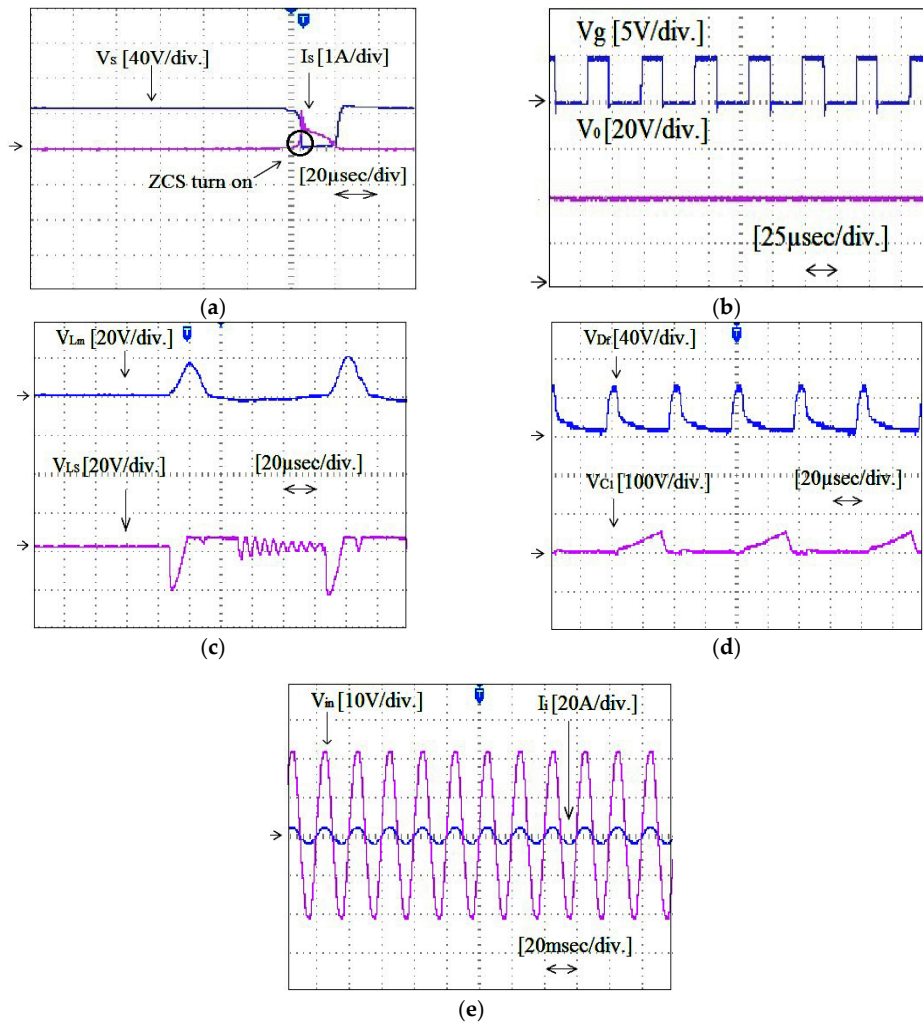


Figure 6. Measured waveforms for the proposed converter (a)  $V_S$  and  $I_S$  (b)  $V_g$  and  $V_0$  (c) voltage across  $L_m$  and  $L_S$  (d) voltage across  $D_f$  and  $C_1$  and (e)  $V_{in}$  and  $I_i$ .

**Table 1.** Component values for the experimental ac-dc PFC converter with proposed passive snubber.

Component	Company	ac-dc PFC Converter with Proposed Passive Snubber
$L_m$	JIME	200 $\mu$ H
$C_0$	nichicon	90 $\mu$ F
$L_S$	-	70 $\mu$ H
$C_1$	Jb	4.3 nF
$C_2$	nichicon	2.5 $\mu$ F
Rectifier Diode	MULTICOMP	1N5408 ( $V_{rrm} = 1000V, I_f(max) = 1 A$ )
MOSFET	FAIRCHILD	IRF840 N-Channel Power MOSFETs, 8A, 450 V/500 V
High Frequency Diode	MIC	BA157 ( $V_{rrm} = 400V, I_{avg} = 1 A$ )
Transformer	JIME	Ferrite Core
Input Inductor	JIME	Ferrite Core
PIC Controller Chip	MICROCHIP	16F877A
Optocoupler IsolationChip	Fairchild semiconductor	MCT2E

The snubber elements  $C_1, D_2, C_2, L_S$  along with  $S$  create a resonant path when  $D_2$  is turned ON. This reduces the turn ON  $di_{D_f}/dt$  of  $S$ . The anode voltage is decreased from the final value  $V_0$  to 0 V. Thus  $L_S$  and  $D_2$  reduces the reverse recovery current of boost diode to a greater extent. When  $V_{C1} V_{C1}$  increases from 0 V to  $V_0, I_{D_f} = 0 A$  and  $V_{D_f}$  decreases from  $V_0$  to 0 V when  $S$  is turned off as in mode 4. There is no additional voltage stress on the main diode and also the reverse-recovery problems are less severe since it achieves soft switching. Figure 6e confirms that the input voltage and input current are in-phase with near unity power factor.

The measured efficiency is about 97%, which is clear from the measured input/output current and voltage waveforms. The ac-dc PFC boost converter is needed to provide sufficient voltage of 400–600 V dc for battery charger in electric vehicle. A prototype circuit is designed to produce a constant dc output  $V_0 = 40 V$  for an input voltage  $V_{in}$  range of  $24 V \pm 10\%$ . It was operated at  $f_s$  of 20 kHz. The boost converter circuit was built using the following components  $L_m = 200 \mu H$ ;  $C_0 = 90 \mu F$ . The Figures 7–11 have been drawn with the help of simulation work carried out in MATLAB for the developed circuit. This has been done to verify the effectiveness of the proposed circuit in terms of efficiency for changes in the input voltage, variation of snubber component values, duty cycle and load respectively for Plug-in-Hybrid Electric vehicle applications. The power efficiency values of the proposed and conventional boost converters are compared at  $P_0 = 75 W, 100 W$  and  $125 W$  (Figure 7). The power efficiency of the proposed one at an ac voltage of  $V_{in} = 24 V$  is 97% at  $P_0 = 75 W, 96.8\%$  at  $P_0 = 100 W$  and  $95.5\%$  at  $P_0 = 125 W$  which is 3.7%, 4% and 4.2% greater than the conventional circuit, respectively. The proposed PFC converter has higher efficiency over wide input and load ranges than the conventional one.

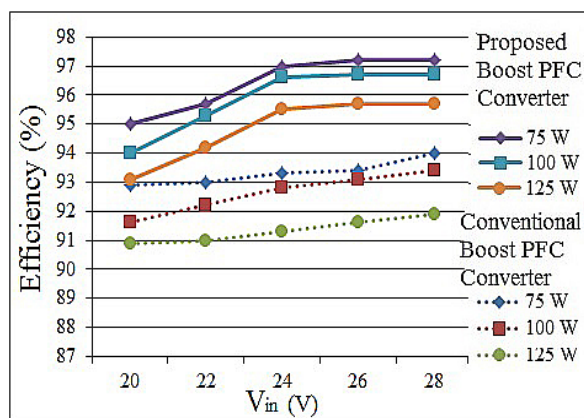


**Figure 7.** Input voltage and efficiency.

The snubber circuit parameter values  $L_s$ ,  $C_1$  and  $C_2$  are varied by  $\pm 20\%$  from the designed values and the power efficiency of the proposed converter is measured at an ac voltage of  $V_{in} = 24$  V, output dc voltage of  $V_0 = 40$  V and  $P_0 = 75$  W, 100 W and 125 W (Figure 8). At the designed range, the efficiency is higher and it is decreased by 0.5% at  $\pm 20\%$  variation. The duty cycle and the power efficiency values of the proposed and conventional converters are plotted at  $P_0 = 75$  W, 100 W and 125 W. During the entire duty cycle range, the proposed one has higher efficiency than the conventional one (Figure 9).

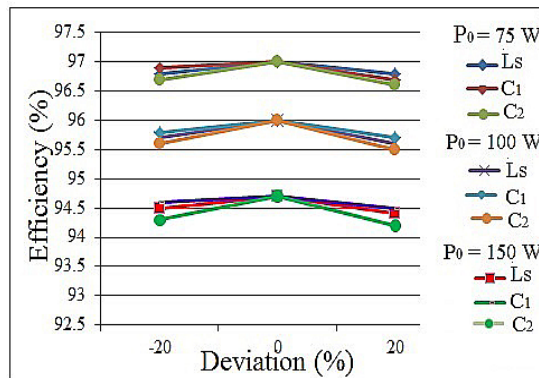


Figure 8. Deviation and efficiency.

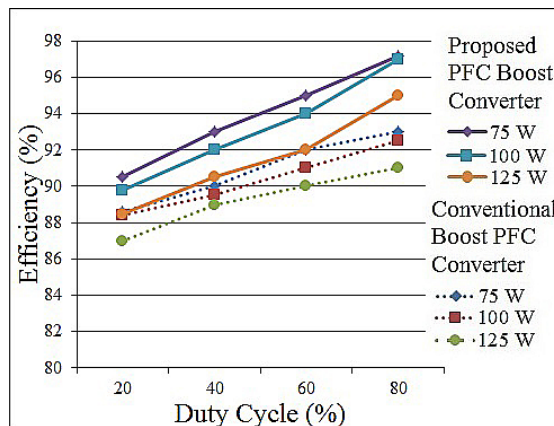


Figure 9. Duty cycle and efficiency.

The output power  $P_0$  is varied from 75 W to 100 W and the circuit efficiency is measured at an ac input voltage of  $V_{in} = 24$  V, output dc voltage of  $V_0 = 40$  V and  $f_s = 20$  kHz (Figure 10). The efficiency decreases when the output power  $P_0$  is increased for both conventional and proposed PFC converters. During the entire operating range the proposed circuit has higher efficiency of more than 6% than that of the conventional one. At  $V_0 = 400$  V,  $f_s = 20$  kHz and  $P_0 = 300$  W the simulation is carried out. The measured efficiency and duty cycle is plotted against input voltage for both proposed and conventional boost PFC converters (Figure 11). The efficiency is 87% for the proposed converter for duty cycle  $> 0.4$  and for duty cycle  $< 0.4$  it is 97%. It is clear that when duty cycle increases efficiency decreases due to the increased conduction losses. Because of this the power conversion efficiency of the proposed converter is high when it operates at duty cycle = 0.4. Table 2 presents the comparison between the conventional and proposed ac-dc boost PFC converter for different parameters.

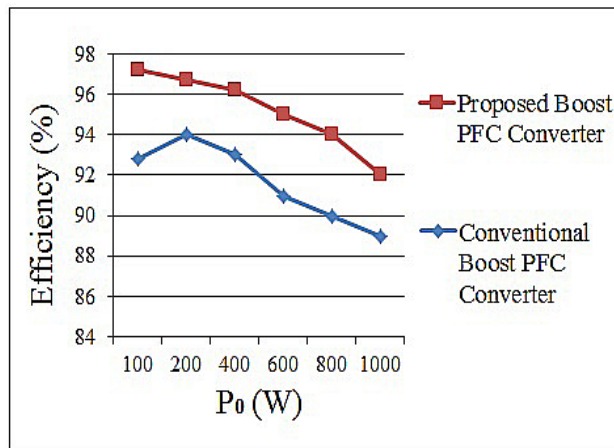


Figure 10. Output power and efficiency.

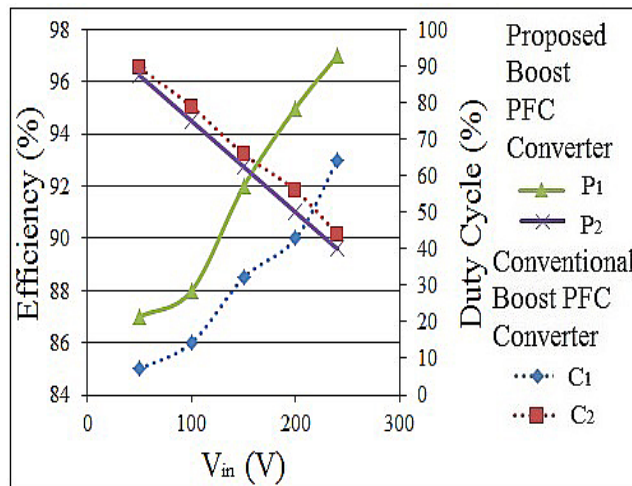


Figure 11. Input voltage and efficiency and duty cycle.

Table 2. Performance comparison of the proposed PFC converter and the conventional PFC converters.

Circuit Type	Switching Features	Components Count	Power Factor	Efficiency (%)
Conventional Boost PFC	Hard Switching	No extra Component	0.9641	91.18
Boost PFC Passive snubber [33]	S—ZCS turn ON and ZVS turn OFF	2 inductor 1 Diode 1 capacitor	0.98	95
Boost PFC Passive snubber [34]	S—ZCS turn ON and turn OFF	2 inductor 2 Diode 1 capacitor	0.9897	95.3
Boost PFC Converter with proposed passive snubber	S—ZCS turn ON and ZVS turn OFF	2 inductor 2 Diode 1 capacitor	0.9897	97

Based on the simulation results, the efficiency and power factor of proposed boost rectifier is compared with the conventional circuit with same circuit ratings. The conventional boost circuit works with an efficiency of about 91% while it is 97% for the proposed boost rectifier with near unity power factor. At rated output power, the efficiency of the proposed ZCS boost PFC converter is about 6% higher than the conventional PFC boost converter. The merits obtained are the increased

overall circuit efficiency, near unity power factor, low voltage switch stresses and high voltage gain with small duty ratio at higher switching frequencies. Figure 8 reveals that at all output load levels the proposed converter achieves a near unity power factor which is comparatively higher than the conventional converters. A grid-stabilization system generally consists of a charging/discharging device which would consist of ten lithium-ion battery boards stacked in parallel and connected to one inverter. For such systems the rechargeable charger for Battery Electric Vehicle (BEV) with the proposed passive snubber can also be applied since it has higher efficiencies at light loads and low ac input lines with minimized charger sizes and charging times [47].

## 6. Conclusions

In this paper a passive snubber for battery charging systems has been designed and developed. The converter switch is turned ON at zero current and turned OFF at zero voltage by the passive snubber. It has reduced the turn ON and turn OFF losses of the boost switch in the ac-dc PFC converter of the charger system. The advantages features of the proposed converter are higher efficiencies at light loads, minimized charger size and charging time and fewer amounts of cost and electricity drawn from the utility. The power conversion efficiency is measured as 97% at an operating condition of  $V_{in} = 24$  V,  $V_0 = 40$  V,  $P_0 = 100$  W and  $f_s = 20$  kHz such that it increases the efficiency by about 6%. Hence the use of the proposed circuit is recommended in battery chargers for increasing the reliability of the boost switch and also in other high power and high frequency applications.

**Conflicts of Interest:** The authors declare no conflict of interest.

## Nomenclature

$d$	Switching duty cycle for the proposed converter.
$D$	Diode.
$C$	Capacitance (F).
$t$	Time (s).
$t_r$	Rise time of the switch current (s).
$t_f$	Fall time of the switch current (s).
$T_{on}$	On-time of the main switch (s).
$R$	Resistance of load resistor ( $\Omega$ ).
$L_S$	Inductance of the snubber inductor of the passive circuit (H).
$f_s$	Switching frequency (Hz).
$S$	Main switch.
$L_m$	Inductance of main inductor (H).
$D_f$	Output diode of the boost converter.
$C_0$	Capacitance of output capacitor of the boost converter (F).
$C_p$	Parasitic capacitance of the switch (F).
$V_{in}$	Input ac voltage of the source (V).
$V_{dc}$	Input dc voltage of the boost converter (V).
$V_0$	Output dc voltage of the ac-dc boost PFC converter (V).
$V_{C1}$	Instantaneous voltage across the snubber capacitor $C_1$ (V).
$V_{C2}$	Instantaneous voltage across the snubber capacitor $C_2$ (V).
$V_g$	Gate to source voltage of the main switch $S$ (V).
$V_{Lm}$	Instantaneous voltage across the main inductor $L_m$ (V).
$V_{Ls}$	Instantaneous voltage across the snubber inductor $L_s$ (V).
$V_{Df}$	Instantaneous voltage of the output diode $D_f$ (V).

$V_S$	Instantaneous voltage across the main switch $S$ (V).
$I_i$	Input ac current of the single phase ac source (A).
$I_0$	Output dc current of the ac-dc boost PFC converter (A).
$I_{Lm}$	Instantaneous current of the main inductor $L_m$ (A).
$I_{Ls}$	Instantaneous current of the snubber inductor $L_s$ (A).
$I_{Df}$	Instantaneous current of the output diode $D_f$ (A).
$I_{D1}$	Instantaneous current of the snubber diode $D_1$ (A).
$I_{D2}$	Instantaneous current of the snubber diode $D_2$ (A).
$I_S$	Instantaneous current of the main switch $S$ (A).
$\Delta I_L$	Current ripple of the main inductor $L_m$ (A).
$P_o$	Output power of the ac-dc boost PFC converter (W).
$\omega_r$	Resonant angular frequency (rad/sec).

#### List of Acronyms

PFC	Power Factor Correction
ac	alternating current
dc	direct current
ac-dc	alternating current to direct current
ZCS	Zero Current Switching
ZVS	Zero Voltage Switching
ZC-ZVS	Zero Current- Zero Voltage Switching
MOSFET	Metal Oxide Semiconductor Field Effect Transistor
EMI	Electro Magnetic Interference
RCD	Circuit composed of a resistor R, a capacitor C and a diode D
PEV	Plug-in-Electric Vehicle
PHEV	Plug-in Hybrid Electric Vehicle
EV	Electric Vehicle
THD	Total Harmonic Distortion
RM	Ripple Mirror
CCM	Continuous Conduction Mode
LCD	Circuit composed of an inductor L, a capacitor C and a diode D
BEV	Battery Electric Vehicle

#### References

1. Morrow, K.; Karner, D.; Francfort, J. *Plug-in Hybrid Electric Vehicle Charging Infrastructure Review*; U.S. Department of Energy—Vehicle Technologies Program; INL/EXT-08-15058; Idaho National Laboratory: Idaho Falls, ID, USA, 2008.
2. Shi, L.; Meintz, A.; Ferdowsi, M. Single-Phase Bidirectional ac-dc Converters for Plug-in Hybrid Electric Vehicle Applications. In *Proceedings of the IEEE Vehicle Power and Propulsion Conference*, Harbin, China, 3–5 September 2008; pp. 1–5.
3. Musavi, F.; Eberle, W.; Dunford, W.G. A High-Performance Single-Phase Bridgeless Interleaved PFC Converter for Plug-in Hybrid Electric Vehicle Battery Chargers. *IEEE Trans. Ind. Appl.* **2011**, *47*, 1833–1843. [[CrossRef](#)]
4. Tanoue, K.; Yanagihara, H.; Kusumi, H. Hybrid is a key technology for future automobiles. In *Hydrogen Technology: Mobile and Portable Applications*; Leon, A., Ed.; Springer Science & Business Media: Karlsruhe, Germany, 2008; pp. 235–272.
5. Matthé, R.; Eberle, U. The voltec system: Energy storage and electric propulsion. In *Lithium-Ion Batteries: Advances and Applications*; Pistoia, G., Ed.; Elsevier Science: Oxford, UK, 2014; pp. 151–176.

6. *IEEE Recommended Practices and Requirements for Harmonic Control in Electric Power Systems*; IEEE Std 519-1992; Institute of Electrical and Electronics Engineers: New York, NY, USA, 1992.
7. *IEEE Recommended Practice for Monitoring Electric Power Quality*; IEEE Std 1159; Institute of Electrical and Electronics Engineers: New York, NY, USA, 1995.
8. Huang, T.; Leu, Y.; Chang, Y.; Hou, S. An energy harvester using self-powered feed forward converter charging approach. *Energy* **2013**, *55*, 769–777. [[CrossRef](#)]
9. Punitha, K.; Devaraj, D.; Sakthivel, S. Artificial neural network based modified incremental conductance algorithm for maximum power point tracking in photovoltaic system under partial shading conditions. *Energy* **2013**, *62*, 330–340. [[CrossRef](#)]
10. Bouilouta, A.; Mellit, A.; Kalogirou, S.A. New MPPT method for stand-alone photovoltaic systems operating under partially shaded conditions. *Energy* **2013**, *55*, 1172–1185. [[CrossRef](#)]
11. Tsai, C.T.; Shen, C.L. High efficiency current-doubler rectifier with low output current ripple and high step-down voltage ratio. *IEEE Trans. Ind. Appl.* **2013**, *8*, 182–189. [[CrossRef](#)]
12. Erickson, R.W.; Maksimovic, D. *Fundamentals of Power Electronics*, 2nd ed.; Plenum Publishers: New York, NY, USA, 2001; pp. 1–791.
13. Li, W.; He, X. Review of non-isolated high-step-up DC/DC converters in photovoltaic grid-connected applications. *IEEE Trans. Power Electron.* **2011**, *58*, 1239–1250.
14. Gerard, M.; Poirot-Crouvezier, J.; Hissel, D.; Pera, M. Ripple current effects on PEMFC aging test by experimental and modeling. *J. Fuel Cell Sci. Technol.* **2010**, *8*. [[CrossRef](#)]
15. Miwa, B.A.; Otten, D.M.; Schlecht, M.F. High efficiency power factor correction using interleaving technique. In Proceedings of the IEEE Applied Power Electronics Conference and Exposition, Boston, MA, USA, 23–27 February 1992; pp. 557–568.
16. Huang, X.; Wang, X.; Nergaard, T.; Lai, J.S.; Xu, X.; Zhu, L. Parasitic ringing and design issues of digitally controlled high power interleaved boost converters. *IEEE Trans. Power Electron.* **2004**, *19*, 1341–1352. [[CrossRef](#)]
17. Haroun, R.; Cid-Pastor, A.; El Aroudi, A.; Martinez-Salamero, L. Synthesis of canonical elements for power processing in DC distribution systems using cascaded converters and sliding-mode control. *IEEE Trans. Power Electron.* **2014**, *29*, 1366–1381. [[CrossRef](#)]
18. Maksimovic, D.; Cuk, S. Switching converters with wide DC conversion range. *IEEE Trans. Power Electron.* **1991**, *6*, 151–157. [[CrossRef](#)]
19. Lopez-Santos, O.; Martinez-Salamero, L.; Garcia, G.; Valderrama-Blavi, H.; Mercuri, D.O. Efficiency analysis of a sliding-mode controlled quadratic boost converter. *IET Power Electron.* **2013**, *6*, 364–373. [[CrossRef](#)]
20. Al-Saffar, M.A.; Ismail, E.H.; Sabzali, A.J. Family of ZC-ZVS converters with wide voltage range for renewable energy systems. *Renew. Energy* **2013**, *6*, 32–43. [[CrossRef](#)]
21. Ma, K.; Lee, Y.S. An integrated flyback converter for dc uninterruptible power supply. *IEEE Trans. Power Electron.* **1996**, *11*, 318–327.
22. Zhao, Q.; Lee, F.C. High-efficiency, high step-up DC-DC converters. *IEEE Trans. Power Electron.* **2003**, *18*, 65–73. [[CrossRef](#)]
23. Wu, T.F.; Lai, Y.S.; Hung, J.C.; Chen, Y.M. Boost converter with coupled inductors and buck-boost type of active clamp. *IEEE Trans. Ind. Electron.* **2008**, *55*, 154–162. [[CrossRef](#)]
24. Tseng, K.C.; Liang, T.J. Novel high-efficiency step-up converter. *IEE Proc. Electr. Power Appl.* **2004**, *151*, 182–190. [[CrossRef](#)]
25. Wai, R.J.; Duan, R.Y. High-efficiency dc-dc converter with high voltage gain. *IEE Proc. Electr. Power Appl.* **2005**, *152*, 793–802. [[CrossRef](#)]
26. Liang, T.J.; Chen, S.M.; Yang, L.S.; Chen, J.F.; Ioinovici, A. Ultra-large gain step-up switched-capacitor DC-DC converter with coupled inductor for alternative sources of Energy. *IEEE Trans. Circuit Syst. I* **2012**, *59*, 864–874. [[CrossRef](#)]
27. Fardoun, A.A.; Ismail, E.H. Ultra step-up DC-DC converter with reduced switch stress. *IEEE Trans. Ind. Appl.* **2010**, *46*, 2025–2034. [[CrossRef](#)]
28. Zhao, Y.; Li, W.; He, X. Single-phase improved active clamp coupled-inductor based converter with extended voltage doubler cell. *IEEE Trans. Power Electron.* **2012**, *27*, 2869–2878. [[CrossRef](#)]

29. Aiswariya, S.; Dhanasekaran, R. Power Factor Correction Converter with an Active Snubber. In Proceedings of the International Conference on Modern Trends in Science Engineering and Technology, Dubai, UAE, 2–3 December 2013; pp. 71–74.
30. Aiswariya, S.; Dhanasekaran, R. Simulation of a New Active Snubber for Power Factor Correction Converter Applications—A Performance Evaluation. *Int. J. Appl. Eng. Res.* **2015**, *10*, 5600–5605.
31. Aiswariya, S.; Dhanasekaran, R. A New Soft Switched Boost PFC Converter With an Active Snubber. *Int. J. Appl. Eng. Res.* **2015**, *10*, 4325–4330.
32. Aiswariya, S.; Dhanasekaran, R. An AC/DC PFC Converter with Active Soft Switching Technique. *Int. J. Energy Optim. Eng.* **2014**, *3*, 101–121. [[CrossRef](#)]
33. Aiswariya, S.; Dhanasekaran, R. Simulation and Analysis of a Single Phase AC-DC Boost PFC Converter with a Passive Snubber for Power Quality Improvement. In Proceedings of the IEEE International Conference on Advances in Communication Control and Computing Technologies, Tamilnadu, India, 8–10 May 2014; pp. 421–425.
34. Aiswariya, S.; Dhanasekaran, R. Efficiency Analysis of a New Passive Snubber for Battery Charging Applications. In Proceedings of the IEEE International Conference on Communication and Signal Processing, Melmaruvathur, Tamilnadu, India, 2–4 April 2015; pp. 17–22.
35. Irving, B.; Jovanovic, M. Analysis, design, and performance evaluation of flying-capacitor passive lossless snubber applied to PFC boost converter. In Proceedings of the IEEE Applied Power Electronics Conference, Dallas, TX, USA, 10–14 March 2002; pp. 503–508.
36. Mahesh, M.; Panda, A. A high performance single-phase AC-DC PFC boost converter with passive snubber circuit. In Proceedings of the IEEE Energy Conversion Congress and Exposition, Raleigh, NC, USA, 14–20 September 2012; pp. 2888–2894.
37. Wu, H.; He, X. Single phase three-level power factor correction circuit with passive lossless snubber. *IEEE Trans. Power Electron.* **2002**, *17*, 946–953.
38. Jiang, S.-G.; Liu, G.-H.; Wang, W.; Xu, D.G. Research on bridgeless boost PFC with soft-switching. In Proceedings of the IEEE Vehicle Power and Propulsion Conference, Dearborn, MI, USA, 7–10 September 2009; pp. 1461–1464.
39. Hwu, K.I.; Tsai, C.L.; Lin, K.F. A simple passive ZCS circuit for PFC converter. In Proceedings of the IEEE Applied Power Electronics Conference, Austin, TX USA, 24–28 February 2008; pp. 1022–1026.
40. Schenk, K. Non Dissipative Snubber Circuit with Saturable Reactor. *U.S. Patent 7, 233, 507*, 19 June 2007.
41. Joung, G.; Ma, K.; Kim, Y. Battery discharger applications of high frequency boost converter with lossless snubber. In Proceedings of the IEEE Power Electronics Specialists Conference, Cairns, Queensland Australia, 23–27 June 2002; pp. 938–942.
42. Li, R.T.H.; Chung, H.S.-H.; Sung, A.K.T. Passive lossless snubber for boost PFC with minimum voltage and current stress. *IEEE Trans. Power Electron.* **2010**, *25*, 602–613. [[CrossRef](#)]
43. Lai, C.-M.; Yang, M.-J.; Liang, S.-K. A Zero Input Current Ripple ZVS/ZCS Boost Converter with Boundary-Mode Control. *Energies* **2014**, *7*, 6765–6782. [[CrossRef](#)]
44. Locment, F.; Sechilariu, M. Modeling and Simulation of DC Microgrids for Electric Vehicle Charging Stations. *Energies* **2015**, *8*, 4335–4356. [[CrossRef](#)]
45. Wang, C.-S.; Li, W.; Meng, Z.; Wang, Y.-F.; Zhou, J.-G. Three-Phase High-Power and Zero-Current-Switching OBC for Plug-In Electric Vehicles. *Energies* **2015**, *8*, 6672–6704. [[CrossRef](#)]
46. Tsai, C.-T.; Shen, C.-L.; Su, J.-C. A Power Supply System with ZVS and Current-Doubler Features for Hybrid Renewable Energy Conversion. *Energies* **2013**, *6*, 4859–4878. [[CrossRef](#)]
47. Mültin, M.; Allerding, F.; Schmeck, H. Integration of Electric Vehicles in Smart Homes—An ICT-based Solution for V2G Scenarios. In Proceedings of the IEEE PES Innovative Smart Grid Technologies Conference, Washington, DC, USA, 16–18 January 2012; pp. 978–985.



© 2015 by the authors; licensee MDPI, Basel, Switzerland. This article is an open access article distributed under the terms and conditions of the Creative Commons by Attribution (CC-BY) license (<http://creativecommons.org/licenses/by/4.0/>).